

Supporting Information

K₅(W₃O₉F₄)(IO₃): An Efficient Mid-Infrared Nonlinear Optical Compound with High Laser Damage Threshold

Chao Wu,^{†,δ} Lin Lin,^{†,δ} Xingxing Jiang,^{‡,δ} Zheshuai Lin,[‡] Zhipeng Huang,[†] Mark G. Humphrey,[§]
P. Shiv Halasyamani,[¶] and Chi Zhang^{*,†}

[†] China-Australia Joint Research Center for Functional Molecular Materials, School of Chemical Science and Engineering, Tongji University, Shanghai 200092, China

[‡] Key Lab of Functional Crystals and Laser Technology, Technical Institute of Physics and Chemistry, Chinese Academy of Sciences, Beijing 100190, China

[§] Research School of Chemistry, Australian National University, Canberra, ACT 2601, Australia

[¶] Department of Chemistry, University of Houston, Houston, TX 77204-5003, USA

^δThese authors contributed equally.

Table of Contents

Theoretical Calculations

Table S1. Selected bond distances (\AA) of $\text{K}_5(\text{W}_3\text{O}_9\text{F}_4)(\text{IO}_3)$ **1**.

Table S2. Atomic coordinates and equivalent isotropic displacement parameters of **1**.

Table S3. Comparison of the important NLO parameters of some typical IR crystals.

Figure S1. Photograph of crystals of **1**.

Figure S2. Experimental and simulated powder X-ray diffraction patterns of **1**.

Figure S3. Thermogravimetric analysis of **1**.

Figure S4. Measured powder XRD pattern of the residual of **1**.

Figure S5. NLO chromophores in **1** (a). Coordination environment of K atoms in **1** (b).

Figure S6. Octahedral distortions in the three unique metal cations in **1**.

Figure S7. Net polarizations in **1**.

Figure S8. Infrared spectrum of **1**.

Figure S9. Raman spectrum of **1**.

Figure S10. Measured SHG intensity versus the particle sizes of **1**, AgGaS_2 and KTP with 2100 nm laser radiation (a). Oscilloscope traces of the SHG signals of **1**, AgGaS_2 and KTP (105–150 mm) are shown in (b).

Figure S11. Energy dispersive spectroscopy analysis of **1**.

Figure S12. Comparison of the transparent regions of different oxide-/iodate-based NLO materials.

Figure S13. Comparison of relative LDTs of NLO crystals with IR transparency region greater than $10 \mu\text{m}$.

Figure S14. Comparison of the SHG activity (vs KDP) of fluorine-containing iodate-based materials.

Figure S15. Electronic band structure along the highly symmetrical path in the Brillouin zone of **1** (a). Partial density of states projected onto the constituent atoms in **1** (b).

References

Theoretical Calculations: Formulas for the calculation of SHG coefficients.

The formulas to calculate the SHG coefficients were originally proposed by Rashkeev et al.¹ and improved by Lin et al.² The second-order susceptibility χ^{ijk} is expressed as follows:²

$$\chi^{ijk} = \chi^{ijk}(\text{VE}) + \chi^{ijk}(\text{VH}) + \chi^{ijk}(\text{twobands}) \quad (1)$$

where $\chi^{ijk}(\text{VE})$ and $\chi^{ijk}(\text{VH})$ denote the contributions from virtual-electron processes and virtual-hole processes, respectively, and $\chi^{ijk}(\text{two bands})$ gives the contribution from two-band processes to χ^{ijk} . The formulas for calculating $\chi^{ijk}(\text{VE})$, $\chi^{ijk}(\text{VH})$ and $\chi^{ijk}(\text{two bands})$ are as follows:

$$\chi^{ijk}(\text{VE}) = \frac{e^3}{2\pi^2 m^3} \sum_{vc} \int \frac{d^3 k^u}{4\pi^3} P(ijk) \text{Im}[p_{vc}^i p_{cc'}^j p_{c'v}^k] \left(\frac{1}{\omega_{cv}^3 \omega_{vc'}^2} + \frac{2}{\omega_{vc}^4 \omega_{c'v}^2} \right) \quad (2)$$

$$\chi^{ijk}(\text{VH}) = \frac{e^3}{2\pi^2 m^3} \sum_{vv'c} \int \frac{d^3 k^u}{4\pi^3} P(ijk) \text{Im}[p_{vv'}^i p_{v'c}^j p_{cv}^k] \left(\frac{1}{\omega_{cv}^3 \omega_{v'c}^2} + \frac{2}{\omega_{vc}^4 \omega_{cv'}^2} \right) \quad (3)$$

$$\chi^{ijk}(\text{twobands}) = \frac{e^3}{\pi^2 m^3} \sum_{vc} \int \frac{d^3 k^u}{4\pi^3} P(ijk) \frac{\text{Im}[p_{vc}^i p_{cv}^j (p_{vv}^k - p_{cc}^k)]}{\omega_{vc}^5} \quad (4)$$

Herein, i , j and k are Cartesian components, v and v' denote VB, and c and c' denote CB. $P(ijk)$ denotes full permutation. The band energy difference and momentum matrix elements between the electronic states m and n are denoted by ω_{mn} and p_{mn}^α , respectively, and they are all implicitly k -point (k^u) dependent. From this sum-over-states formula the SHG coefficient component d_{ijk} ($= 1/2\chi^{ijk}$) is determined.

Table S1. Selected bond distances (\AA) of $\text{K}_5(\text{W}_3\text{O}_9\text{F}_4)(\text{IO}_3)$ ^a.

W(1)-O(8)	1.742(13)	W(1)-O(7)	1.750(13)	W(1)-O(9)#1	1.889(2)
W(1)-O(9)	1.889(2)	W(1)-F(4)	2.094(11)	W(1)-O(4)	2.201(12)
W(2)-O(4)	1.785(12)	W(2)-O(5)	1.767(12)	W(2)-O(6)#1	1.892(4)
W(2)-O(6)	1.892(4)	W(2)-F(3)	2.033(12)	W(2)-O(2)	2.09(2)
W(3)-O(1)	1.757(15)	W(3)-O(2)	1.82(2)	W(3)-O(3)	1.885(4)
W(3)-O(3)#1	1.885(4)	W(3)-F(1)	1.902(14)	W(3)-F(2)	2.071(13)
I(1)-O(10)	1.822(12)	I(1)-O(11)	1.986(15)	I(1)-O(12)	1.980(16)
K(1)-F(3)#13	2.677(10)	K(1)-O(2)	3.37(2)	K(1)-O(8)	2.760(11)
K(1)-O(11)#7	2.645(16)	K(1)-O(1)#13	2.939(12)	K(1)-O(6)#14	3.20(2)
K(2)-O(2)#6	3.34(2)	K(2)-O(4)#6	2.891(11)	K(2)-F(4)#6	2.744(10)
K(2)-F(2)#6	2.783(10)	K(2)-O(12)#10	2.748(16)	K(2)-O(6)	3.30(3)
K(2)-O(3)	3.26(3)	K(2)-O(9)	3.010(14)	K(3)-F(1)#13	2.716(12)
K(3)-F(3)#15	2.857(10)	K(3)-O(5)#15	3.183(16)	K(3)-O(10)	2.937(12)
K(3)-O(11)	2.797 (18)	K(4)-F(2)	2.807(10)	K(4)-F(1)	3.343(16)
K(4)-O(5)#11	2.789(12)	K(4)-O(7)#11	2.848(12)	K(4)-O(3)	3.29(2)
K(5)-F(4)	2.691(10)	K(5)-O(1)#13	2.952(12)	K(5)-O(8)	3.351(17)
K(5)-O(9)	3.175(16)	K(5)-O(10)#6	2.740(12)	K(5)-O(12)#10	3.201(17)

^a Symmetry codes for $\text{K}_5(\text{W}_3\text{O}_9\text{F}_4)(\text{IO}_3)$: #1 x,y-1,z; #2 x,y,z+1; #3 x,y-1,z+1; #4 x+1,y,z+1; #5 x+1,y-1,z+1; #6 x,y+1,z; #7 x+1,y,z; #8 x+1,y-1,z; #9 x,-y,z; #10 x,-y+1,z; #11 x-1,y,z; #12 x+1,-y+1,z; #13 x,y+1,z-1; #14 x,y,z-1; #15 x-1,y,z-1; #16 x-1,y+1,z-1; #17 x-1,y+1,z.

Table S2. Atomic coordinates and equivalent isotropic displacement parameters of K₅(W₃O₉F₄)(IO₃).

Atom	x	y	z	U _{eq} (Å ²)	occ	BVS
K(1)	6540(5)	5000	1591(6)	38(1)	0.5	1.27
K(2)	3960(6)	5000	6528(6)	42(1)	0.5	1.38
K(3)	102(7)	5000	704(6)	39(1)	0.5	1.15
K(4)	286(7)	5000	7155(8)	55(2)	0.5	1.17
K(5)	3551(8)	5000	3076(6)	47(1)	0.5	1.15
W(1)	6669(1)	0	5059(1)	30(1)	0.5	6.25
W(2)	7141(1)	0	8582(1)	33(1)	0.5	6.33
W(3)	3476(1)	0	9533(1)	35(1)	0.5	6.42
I(1)	332(2)	0	3839(2)	59(1)	0.5	3.74
F(1)	1558(15)	0	9676(15)	76(6)	0.5	1.16
F(2)	2499(12)	0	7664(12)	46(3)	0.5	0.98
F(3)	7826(12)	0	10467(11)	36(2)	0.5	1.08
F(4)	4474(12)	0	4833(11)	40(3)	0.5	1.05
O(1)	4141(15)	0	11152(14)	37(3)	0.5	2.00
O(2)	5160(30)	0	9060(20)	75(5)	0.5	2.09
O(3)	3210(30)	5000	9290(20)	74(7)	0.5	2.30
O(4)	6294(13)	0	6972(11)	37(3)	0.5	2.17
O(5)	8893(16)	0	8366(17)	89(9)	0.5	1.97
O(6)	6840(20)	5000	8740(19)	56(4)	0.5	2.26
O(7)	8495(13)	0	5610(13)	37(3)	0.5	1.88
O(8)	6481(19)	0	3443(12)	47(4)	0.5	2.06
O(9)	6354(11)	5000	5170(15)	31(3)	0.5	2.33
O(10)	1430(14)	0	2678(13)	41(3)	0.5	1.97
O(11)	-887(16)	3780(40)	2890(15)	34(3)	0.5	1.46
O(12)	1435(16)	3710(50)	4918(14)	34(3)	0.5	1.42

Table S3. Comparison of the important NLO parameters of some typical IR crystals.

Compound	Space group	SHG response (\times KDP)	LDT (\times AGS)	IR transparency edge (μm)
AgGaS ₂ (AGS) ³	<i>I</i> -42 <i>d</i>	25	1	13
LiGaS ₂ ⁴	<i>Pna</i> 2 ₁	10	11	11.6
LiInS ₂ ⁵	<i>Pna</i> 2 ₁	15	2.5	13.2
BaGa ₄ S ₇ ⁶	<i>Pmn</i> 2 ₁	25	3	13.7
AgGaSe ₂ ⁷	<i>I</i> -42 <i>d</i>	30	5	17
AgGa ₂ PS ₆ ⁸	<i>Cc</i>	25	5.1	16.7
LiGa ₂ PS ₆ ⁹	<i>Cc</i>	12.5	10.4	16.6
LiCd ₃ PS ₆ ⁹	<i>Cc</i>	20	5.5	17.5
CsLiVO ₄ ¹⁰	<i>Cmc</i> 2 ₁	5	28	6
LiIO ₃ ¹¹	<i>P</i> 6 ₃	11.5	3.4	6.5
RbIO ₃ ¹²	<i>R</i> 3 <i>m</i>	20	20	13
RbIO ₂ F ₂ ¹²	<i>Pca</i> 2 ₁	4	32	12
CsIO ₃ ¹³	<i>R</i> 3 <i>m</i>	15	15	5.5
K ₂ BiI ₅ O ₁₅ ¹⁴	<i>Abm</i> 2	3	16	12
Rb ₂ BiI ₅ O ₁₅ ¹⁴	<i>Abm</i> 2	3	13.8	12
NaSb ₃ F ₁₀ ¹⁵	<i>P</i> 6 ₃	3.2	32.5	7.8
Rb ₂ CdBr ₂ I ₂ ¹⁶	<i>Ama</i> 2	4	6	14
Pb ₁₇ O ₈ Cl ₁₈ ¹⁷	<i>Ama</i> 2	4	12.8	13.9
LaSnGa ₅ O ₁₄ ¹⁸	<i>P</i> 321	12	80	7
Li ₂ ZrTeO ₆ ¹⁹	<i>R</i> 3	2.5	44	6
LiNbO ₃ ²⁰	<i>R</i> 3 <i>c</i>	11	3.5	5
KTiOPO ₄ ²¹	<i>Pna</i> 2 ₁	12	15	5.5
K ₅ (W ₃ O ₉ F ₄)(IO ₃) ^a	<i>P</i> <i>m</i>	11	95	10.5

^athis work

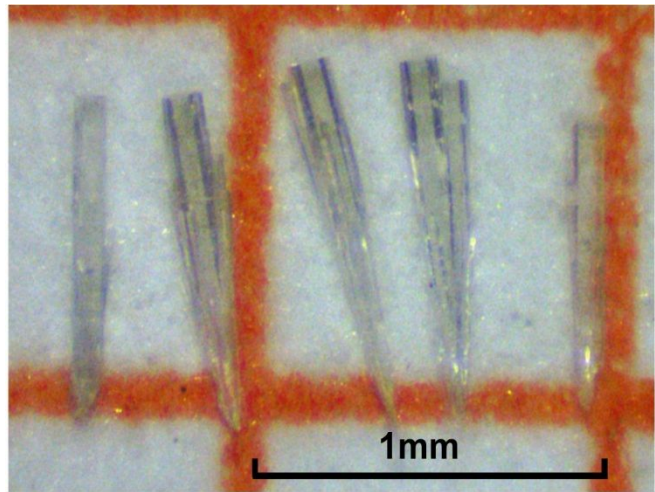


Figure S1. Photograph of crystals of $K_5(W_3O_9F_4)(IO_3)$.

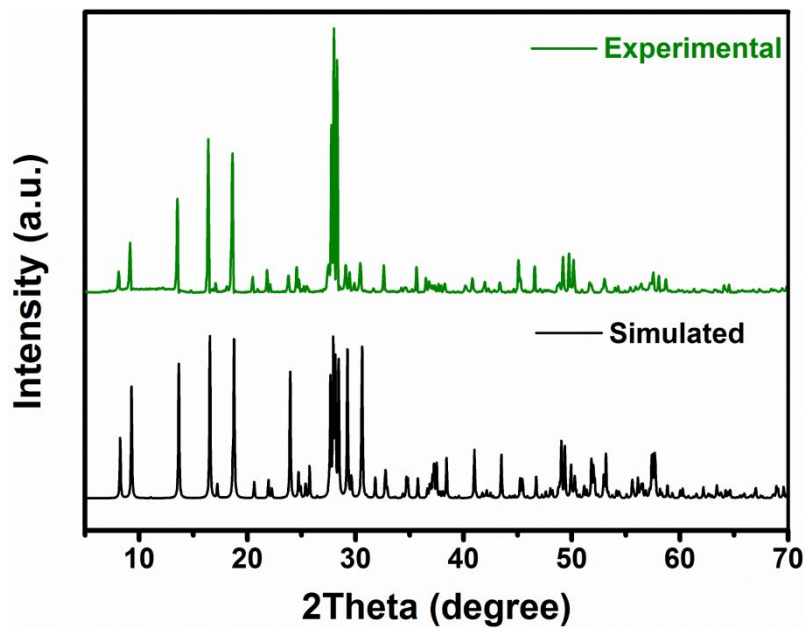


Figure S2. Experimental and simulated powder X-ray diffraction patterns of $\text{K}_5(\text{W}_3\text{O}_9\text{F}_4)(\text{IO}_3)$.

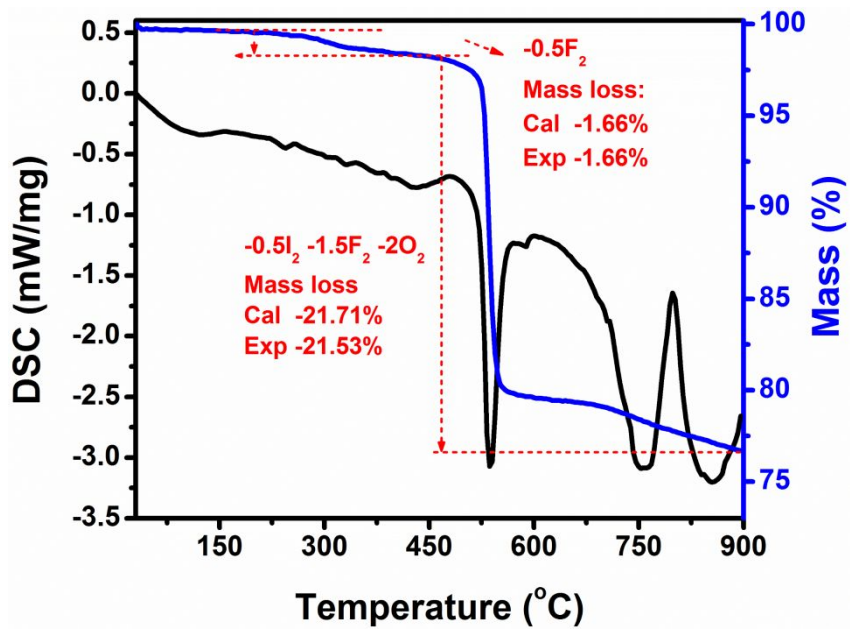


Figure S3. Thermogravimetric analysis of $\text{K}_5(\text{W}_3\text{O}_9\text{F}_4)(\text{IO}_3)$ under a N_2 atmosphere. The thermal stability of $\text{K}_5(\text{W}_3\text{O}_9\text{F}_4)(\text{IO}_3)$ was evaluated by TGA and DSC measurements, the curves showing that $\text{K}_5(\text{W}_3\text{O}_9\text{F}_4)(\text{IO}_3)$ is stable up to 250 °C. There is a slow weight loss starting at 250 °C, with further heating resulting in a sharp weight loss at around 480–570 °C. These weight losses correspond to the release of I₂, O₂, and F₂. The final residues were K_2WO_4 and KI, which was confirmed by powder XRD (Figure S4).

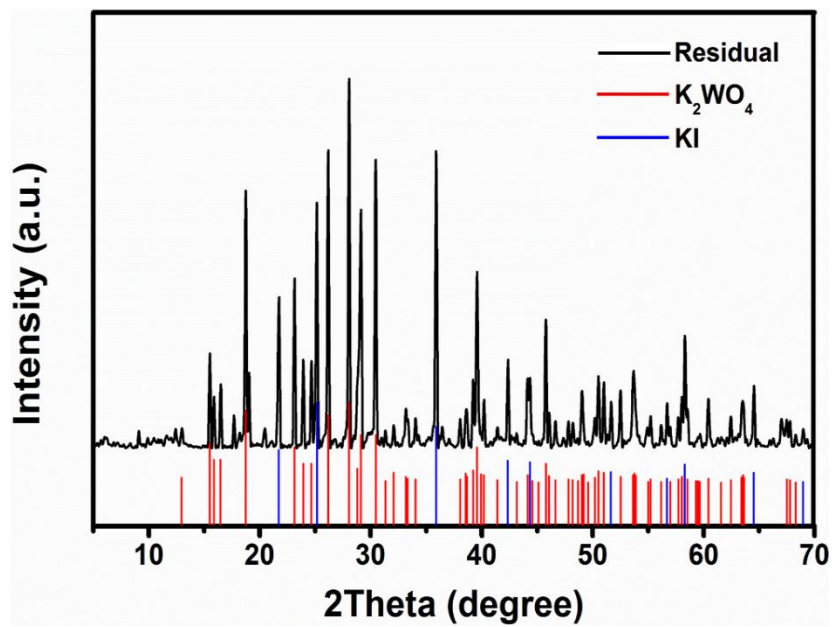


Figure S4. Measured powder XRD pattern of the residual material from $K_5(W_3O_9F_4)(IO_3)$ following thermal treatment.

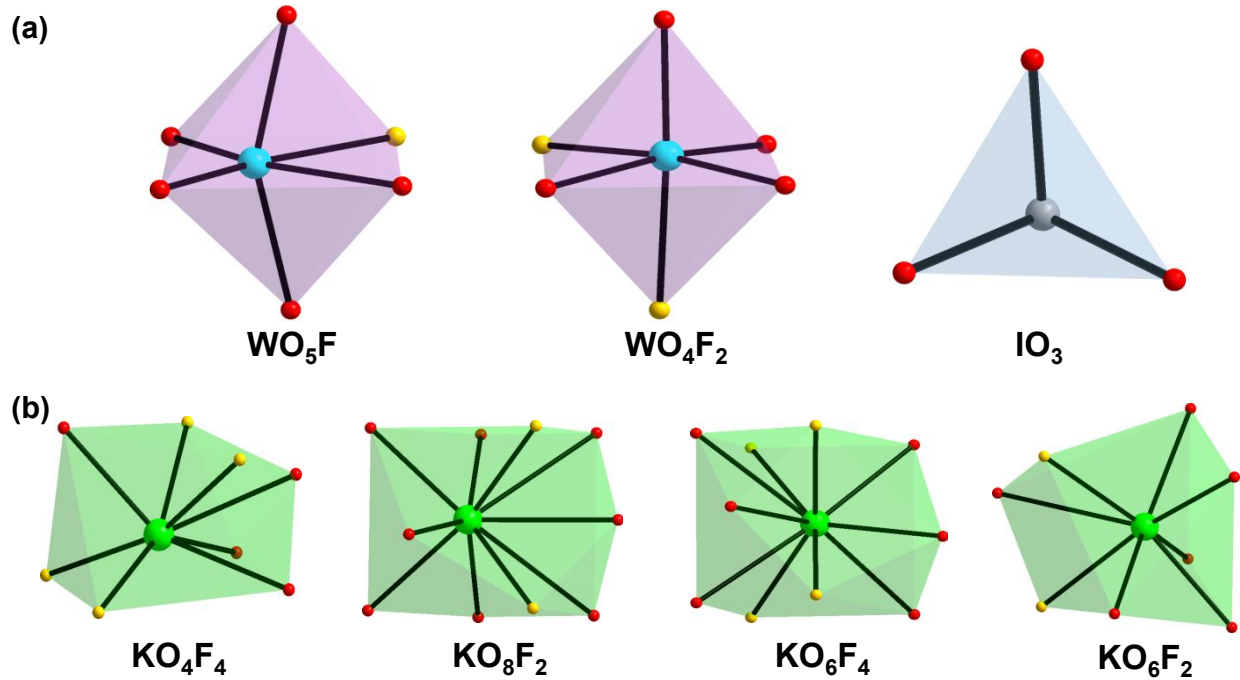


Figure S5. (a) NLO chromophores in $\text{K}_5(\text{W}_3\text{O}_9\text{F}_4)(\text{IO}_3)$. (b) Coordination environment of K atoms in $\text{K}_5(\text{W}_3\text{O}_9\text{F}_4)(\text{IO}_3)$. Color codes: W blue, O red, F yellow, I gray, K green. The K^+ cations are in eight- and ten-coordinated environments, bonded to O/F atoms with $\text{K}-\text{O}/\text{F}$ bond distances in the range of 2.63(3)–3.39(3) Å and 2.670(13)–3.40(2) Å, respectively.

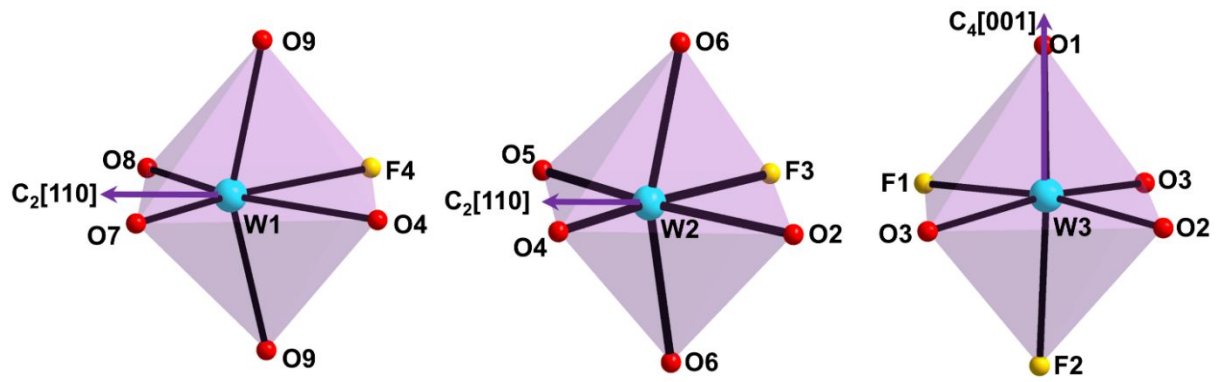


Figure S6. Octahedral distortions in the three unique metal cations in $K_5(W_3O_9F_4)(IO_3)$. The arrows represent the approximate directions of the distortion and polarization. Color codes: W blue, O red, F yellow.

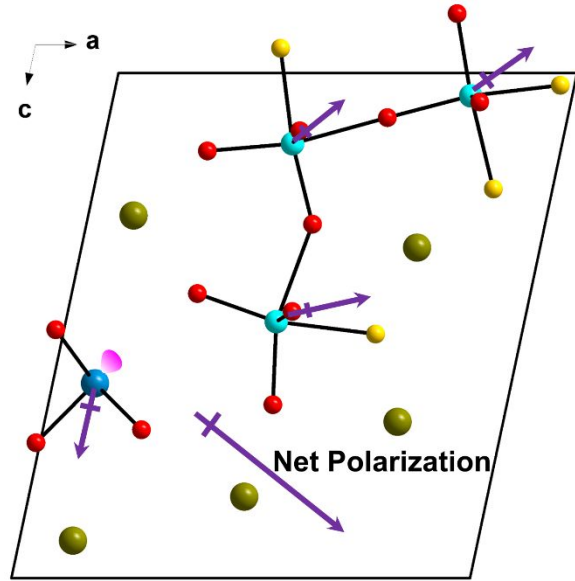


Figure S7. Net polarizations in $K_5(W_3O_9F_4)(IO_3)$.

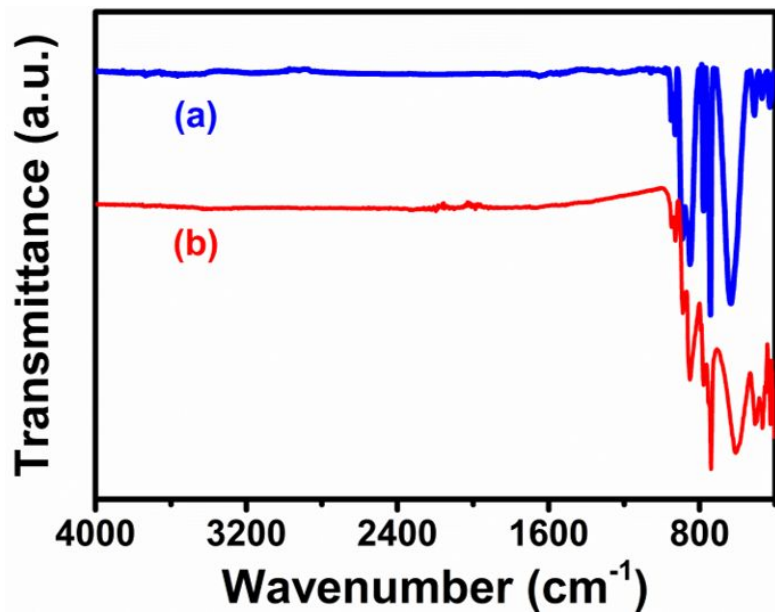


Figure S8. Infrared spectra of $\text{K}_5(\text{W}_3\text{O}_9\text{F}_4)(\text{IO}_3)$ from different samples: (a) crystalline powder mixed with dried KBr in mass ratios of about 1:100; (b) as-grown needle-like crystals.

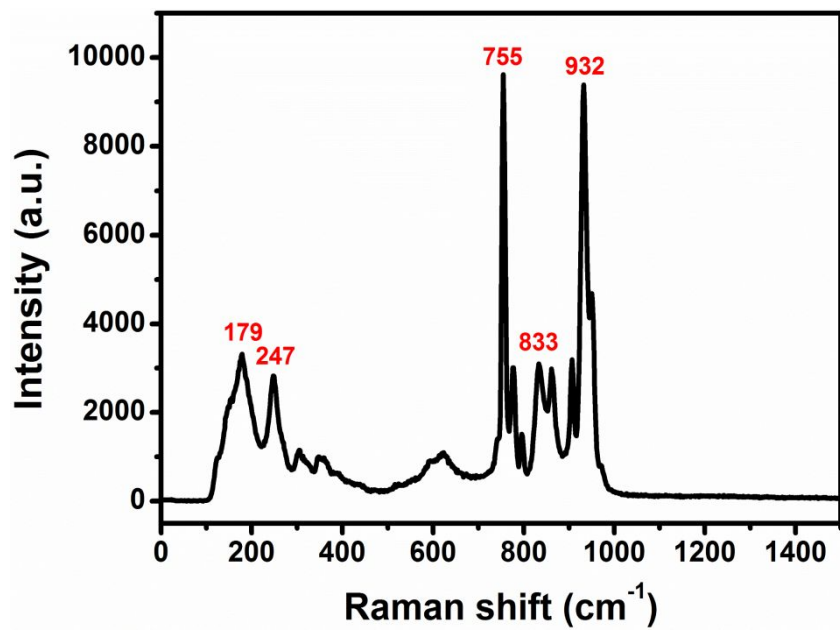


Figure S9. Raman spectrum of $\text{K}_5(\text{W}_3\text{O}_9\text{F}_4)(\text{IO}_3)$.

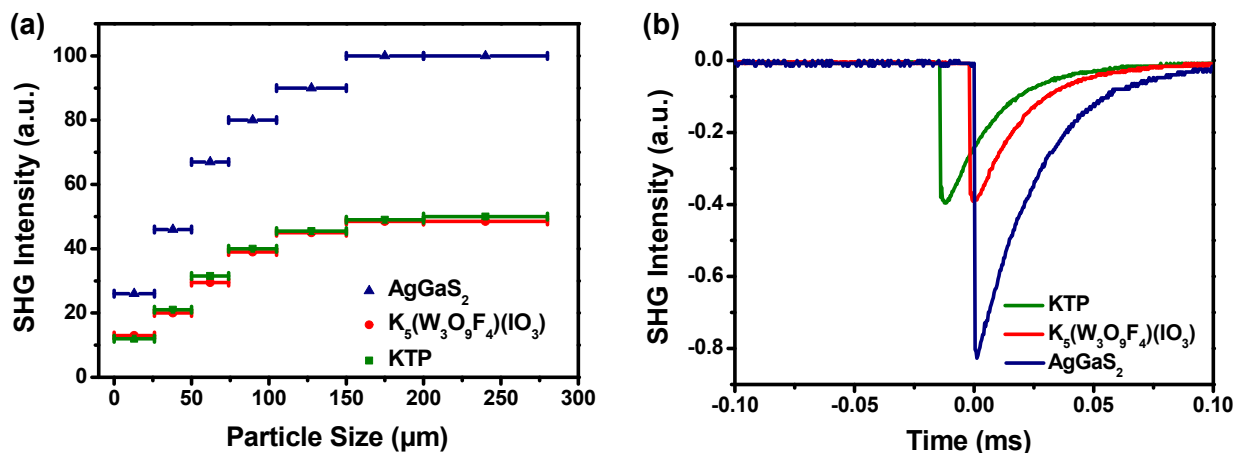


Figure S10. Measured SHG intensity versus the particle sizes of K₅(W₃O₉F₄)(IO₃), AgGaS₂ and KTP with 2100 nm laser radiation (a). Oscilloscope traces of the SHG signals of K₅(W₃O₉F₄)(IO₃), AgGaS₂ and KTP (105–150 mm) are shown in (b).

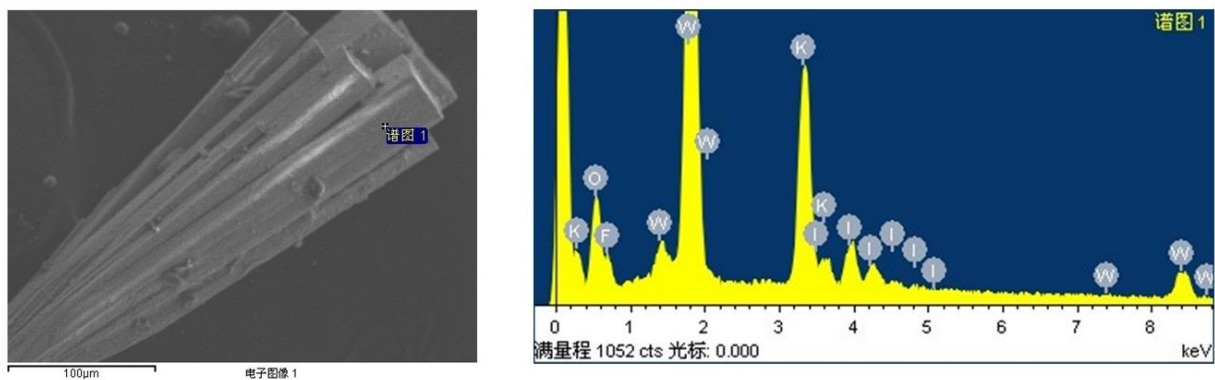


Figure S11. Energy dispersive spectroscopy analysis of $K_5(W_3O_9F_4)(IO_3)$, confirming the K:W:I:O:F elemental composition. The EDS analyses of $K_5(W_3O_9F_4)(IO_3)$ show that the average molar ratio of K:W:I:O:F is 4.75:2.83:1:11.1:3.26, which is consistent with that determined from the single-crystal X-ray structural study.

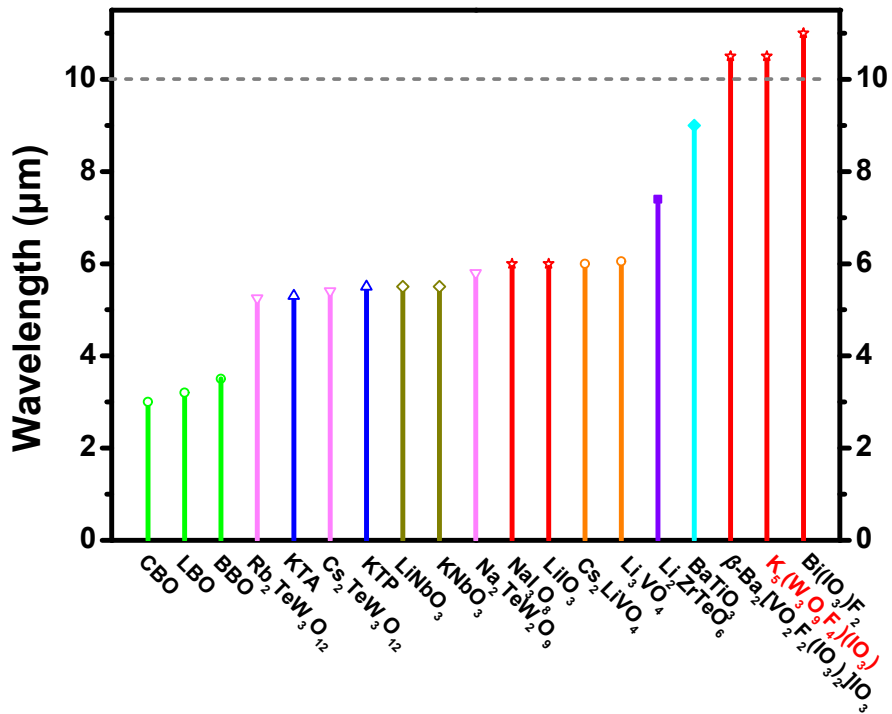


Figure S12. Comparison of the transparent regions of different oxide-/iodate-based NLO materials, including KTP,²¹ Na₂TeW₂O₉,²² BaTiO₃,²³ LiIO₃,¹¹ La₃SnGa₅O₁₄,¹⁸ ZnGeP₂,²⁴ AgGaS₂,³ Bi(IO₃)F₂,²⁵ CBO,³² LBO,³² BBO,³² KTA,³³ Rb₂TeW₃O₁₂,³⁴ Cs₂TeW₃O₁₂,³⁴ LiNbO₃,²⁰ KNbO₃,³⁵ NaI₃O₈,³⁶ Cs₂LiVO₄,¹⁰ Li₂ZrTeO₆,¹⁹ β -Ba₂[VO₂F₂(IO₃)₂](IO₃)³⁷ and K₅(W₃O₉F₄)(IO₃).³⁷

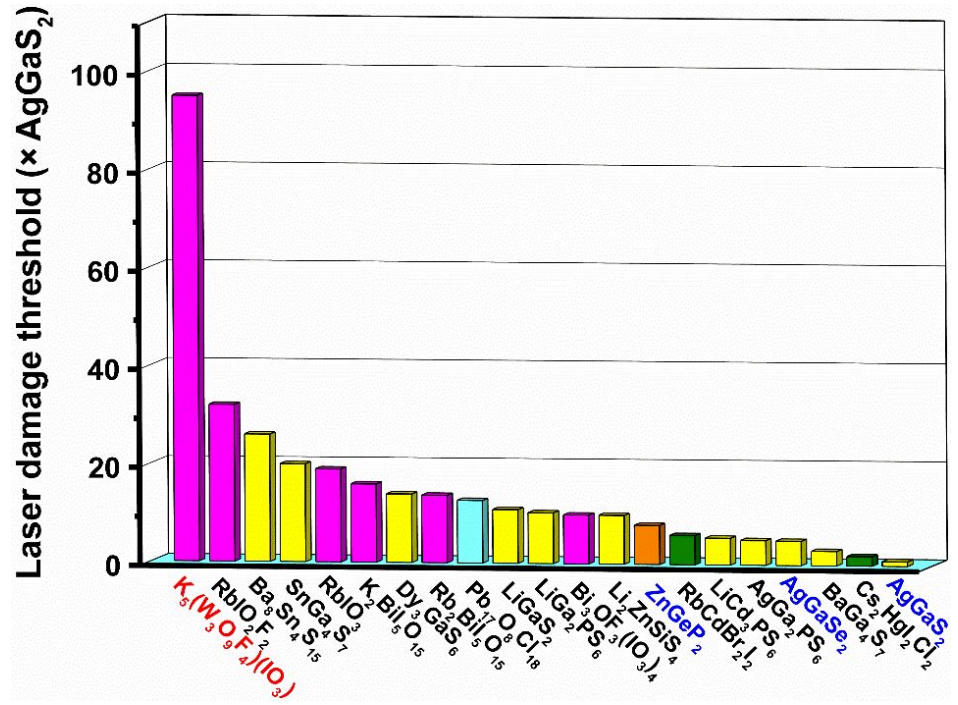


Figure S13. Comparison of relative LDTs of NLO crystals with IR transparency region greater than 10 μm . including AgGaS₂,³ LiGaS₂,⁴ BaGa₄S₇,⁶ AgGaSe₂,⁷ AgGa₂PS₆,⁸ LiGa₂PS₆,⁹ LiCd₃PS₆,⁹ RbIO₃,¹² RbIO₂F₂,¹² K₂Bi₅O₁₅,¹⁴ Rb₂Bi₅O₁₅,¹⁴ Rb₂CdBr₂I₂,¹⁶ Pb₁₇O₈Cl₁₈,¹⁷ ZnGeP₂,²⁴ Bi₃OF₃(IO₃)₄,²⁶ Ba₈Sn₄S₁₅,²⁷ SnGa₄S₇,²⁸ Dy₃GaS₆,²⁹ Li₂ZnSiS₄,³⁰ Cs₂HgI₂Cl₂³¹ and K₅(W₃O₉F₄)(IO₃).

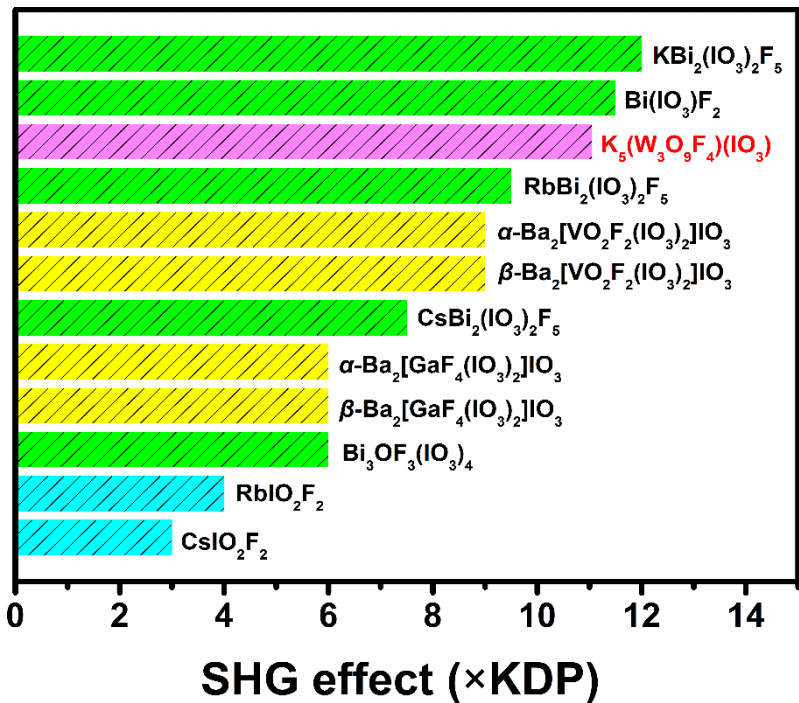


Figure S14. Comparison of the SHG activity (vs KDP) of fluorine-containing iodate-based materials, including RbIO_2F_2 ,¹² CsIO_2F_2 ,¹³ $\text{Bi}_3\text{OF}_3(\text{IO}_3)_4$,²⁶ $\text{Bi}(\text{IO}_3)\text{F}_2$,²⁵ α -/ β - $\text{Ba}_2[\text{VO}_2\text{F}_2(\text{IO}_3)_2]\text{IO}_3$,³⁷ α -/ β - $\text{Ba}_2[\text{GaF}_4(\text{IO}_3)_2]\text{IO}_3$,³⁸ $\text{XBi}_2(\text{IO}_3)_2\text{F}_5$ (X = K, Rb, Cs),³⁹ and $\text{K}_5(\text{W}_3\text{O}_9\text{F}_4)(\text{IO}_3)$.

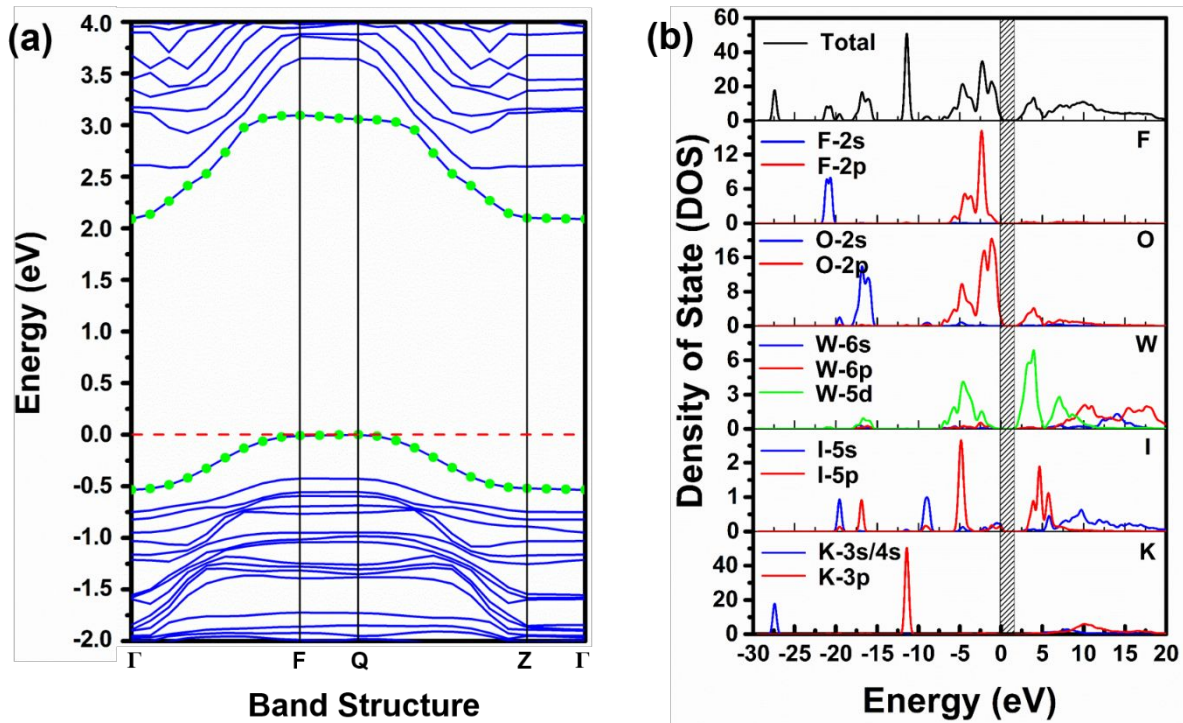


Figure S15. Electronic band structure along the highly symmetrical path in the Brillouin zone of $K_5(W_3O_9F_4)(IO_3)$ (a). Partial density of states projected onto the constituent atoms in $K_5(W_3O_9F_4)(IO_3)$ (b).

References

1. S. N. Rashkeev, W. R. L. Lambrecht, B. Segall, *Phys. Rev. B*, **1998**, *57*, 3905-3919.
2. J. Lin, M. H. Lee, Z. P. Liu, C. T. Chen, C. J. Pickard, *Phys. Rev. B*, **1999**, *60*, 13380-13389.
3. D. S. Chemla, P. J. Kupecek, D. S. Robertson and R. C. Smith, *Opt. Commun.*, **1971**, *3*, 29-31.
4. L. Isaenko, A. Yelisseyev, S. Lobanov, A. Titov, V. Petrov, J. J. Zondy, P. Krinitzin, A. Merkulov, V. Vedenyaoin and J. Smirnova, *Cryst. Res. Technol.*, **2003**, *38*, 379-387.
5. S. Fossier, S. Salaun, J. Mangin, O. Bidault, I. Thenot, J. J. Zondy, W. D. Chen, F. Rotermund, V. Petrov, P. Petrov, J. Henningsen, A. Yelisseyev, L. Isaenko, S. Lobanov, O. Balachninaite, G. Slekys and V. Sirutkaitis, *J. Opt. Soc. Am. B*, **2004**, *21*, 1981-2007.
6. X. Lin, G. Zhang and N. Ye, *Cryst. Growth Des.*, **2009**, *9*, 1186-1189.
7. G. Boyd, H. Kasper, J. McFee and F. Storz, *IEEE J. Quantum Electron.*, **1972**, *8*, 900-908.
8. J. H. Feng, C. L. Hu, X. Xu, B. X. Li, M. J. Zhang and J. G. Mao, *Chem. Eur. J.*, **2017**, *23*, 10978-10982.
9. J. H. Feng, C. L. Hu, B. Li and J. G. Mao, *Chem. Mater.*, **2018**, *30*, 3901-3908.
10. G. Han, Y. Wang, X. Su, Z. Yang and S. L. Pan, *Sci. Rep.*, **2017**, *7*, 1901-1909.
11. W. S. Otaguro, E. Wiener-Avnear and S. P. S. Porto, *Appl. Phys. Lett.*, **1971**, *18*, 499-501.
12. Q. Wu, H. M. Liu, F. C. Jiang, L. Kang, L. Yang, Z. S. Lin, Z. H. Hu, X. G. Chen, X. G. Meng and J. J. Qin, *Chem. Mater.*, **2016**, *28*, 1413-1418.
13. M. Zhang, C. Hu, T. Abudouwufu, Z. H. Yang and S. L. Pan, *Chem. Mater.*, **2018**, *30*, 1136-1145.
14. Y. Huang, X. G. Meng, P. F. Gong, L. Yang, Z. S. Lin, X. G. Chen and J. J. Qin, *J. Mater. Chem. C*, **2014**, *2*, 4057-4062.
15. G. Zhang, J. J. Qin, T. Liu, Y. J. Li, Y. C. Wu and C. T. Chen, *Appl. Phys. Lett.*, **2009**, *95*, 261104(1)-261104(3).
16. Q. Wu, X. G. Meng, C. Zhong, X. G. Chen and J. G. Qin, *J. Am. Chem. Soc.*, **2014**, *136*, 5683-5686.
17. H. Zhang, M. Zhang, S. L. Pan, X. Y. Dong, Z. H. Yang, X. L. Hou, Z. Wang, K. B. Chang and K. R. Poeppelmeier, *J. Am. Chem. Soc.*, **2015**, *137*, 8360-8363.
18. H. C. Lan, F. Liang, X. X. Jiang, C. Zhang, H. H. Yu, Z. S. Lin, H. J. Zhang, J. Y. Wang and Y. C. Wu, *J. Am. Chem. Soc.*, **2018**, *140*, 4684-4690.
19. W. Q. Lu, Z. L. Gao, X. T. Liu, X. X. Tian, Q. Wu, C. G. Li, Y. X. Sun, Y. Liu and X. T. Tao, *J. Am. Chem. Soc.*, **2018**, *140*, 13089-13096.
20. G. D. Boyd, R. C. Miller, K. Nassau, W. L. Bond and A. Savage, *Appl. Phys. Lett.*, **1964**, *5*, 234-236.
21. M. E. Hagerman and K. R. Poeppelmeier, *Chem. Mater.*, **1995**, *7*, 602-621.
22. W. G. Zhang, F. Li, S. H. Kim and P. S. Halasyamani, *Cryst. Growth Des.*, **2010**, *10*, 4091-4095.
23. P. Becker, *Adv. Mater.*, **1998**, *10*, 979-992.
24. G. D. Boyd, E. Buehler and F. G. Storz, *Appl. Phys. Lett.*, **1971**, *18*, 301-304.
25. F. F. Mao, C. L. Hu, X. Xu, D. Yan, B. P. Yang and J. G. Mao, *Angew. Chem. Int. Ed.*, **2017**, *56*, 2151-2155.
26. M. Zhang, X. Su, M. Mutailipu, Z. H. Yang and S. L. Pan, *Chem. Mater.*, **2017**, *29*, 945-949.
27. Z. Z. Luo, C. S. Lin, W. L. Zhang, H. Zhang, Z. Z. He and W. D. Cheng, *Chem. Mater.*, **2014**, *26*, 1093-1099.
28. Z. Z. Luo, C. S. Lin, H. H. Cui, W. L. Zhang, H. Zhang, Z. Z. He and W. D. Cheng, *Chem. Mater.*, **2014**, *26*, 2743-2749.

29. M. J. Zhang, B. X. Li, B. W. Liu, Y. H. Fan, X. G. Li, H. Y. Zeng and G. C. Guo, *Dalton Trans.*, **2013**, *42*, 14223-14229.
30. G. M. Li, Y. Chu and Z. X. Zhou, *Chem. Mater.*, **2018**, *30*, 602-606.
31. G. Zhang, Y. J. Li, K. Jiang, H. Y. Zeng, T. Liu, X. G. Chen, J. G. Qin, Z. S. Lin, P. Z. Fu, Y. C. Wu and C. T. Chen, *J. Am. Chem. Soc.*, **2012**, *134*, 14818-14822.
32. P. Becker, *Adv. Mater.* **1998**, *10*, 979-992.
33. J. D. Bierlein and H. Vanherzele, *Appl. Phys. Lett.*, **1989**, *54*, 783-785.
34. J. Goodey, K. M. Ok, J. Broussard, C. Hofmann, F. V. Escobedo and P. S. Halasyamani, *J. Solid State Chem.*, **2003**, *175*, 3-12.
35. T. Fukuda and Y. Uematsu, *Jpn. J. Appl. Phys.* **1972**, *11*, 163-169.
36. D. Phanon and I. Gautier-Luneau, *Angew. Chem. Int. Ed.* **2007**, *46*, 8488-8491.
37. H. W. Yu, M. L. Nisbet and K. R. Poepelmeier, *J. Am. Chem. Soc.* **2018**, *140*, 8868-8876.
38. J. Chen, C. L. Hu, F. F. Mao, J. H. Feng and J. G. Mao, *Angew. Chem. Int. Ed.* **2019**, *58*, 2098-2102.
39. H. M. Liu, Q. Wu, X. X. Jiang, Z. S. Lin, X. G. Meng, X. G. Chen and J. G. Qin, *Angew. Chem. Int. Ed.* **2017**, *56*, 9492-9496.